Hindawi
International Journal of RF and Microwave Computer-Aided Engineering
Volume 2023, Article ID 8701539, 11 pages
https://doi.org/10.1155/2023/8701539

Research Article

Development of a Broadband and High-Gain Circularly Polarized Array of Multilayer Slot Antennas for X-Band Wireless Communication Networks

Hosein Saghafi, Robab Kazemi, and Hamed Hamlbar Gerami

Faculty of Electrical and Computer Engineering, University of Tabriz, Tabriz, Iran

Correspondence should be addressed to Robab Kazemi; r.kazemi@tabrizu.ac.ir

Received 14 July 2023; Revised 11 September 2023; Accepted 26 September 2023; Published 12 October 2023

Academic Editor: R.K. Mishra

This paper presents a wideband cavity-backed slot antenna array designed for X-band wireless communication systems. The antenna element consists of a circular slot combined with a cross-slotted patch; both are fed by an L-shaped microstrip line through proximity coupling to extend the impedance bandwidth and gain. The reduction of beam squint in the radiation patterns, caused by the asymmetric feed line, is achieved through intelligent optimization of the dimensions and position of the cross slot on the patch. Additionally, a back cavity is included to provide unidirectional radiation and enhance gain. The antenna exhibits right-hand circularly polarized (RHCP) radiation patterns with high gain over a wideband frequency range. To further improve the axial ratio (AR) bandwidth and gain, the antenna is utilized in a 2×2 array configuration with a sequential rotation feed network. The overall dimensions of the proposed array are $1.42\lambda_0 \times 1.42\lambda_0 \times 0.45\lambda_0$, where λ_0 represents the wavelength at the center frequency of 10 GHz. The fabricated array is then tested, and the measurements show an impedance bandwidth of 60% (7 GHz-13 GHz) with $|S_{11}| < -10$ dB, a 3 dB AR bandwidth of 42% (7.45-11.65 GHz), and a peak gain of 11.14 dB. The simulated and measured results exhibit good agreement, validating the effectiveness of the design.

1. Introduction

In modern wireless communication systems, such as satellites, radars, and radio frequency identification (RFID) systems, wideband circularly polarized (CP) antennas are becoming increasingly popular due to their advantages over linearly polarized antennas [1, 2]. CP antennas offer benefits such as reduced sensitivity to Faraday's rotation [3], decreased multipath interference and fading, and reduced polarization mismatch between transmitting and receiving antennas [4–7].

Various types of structures have been developed for designing CP antennas, including dielectric resonator antennas (DRAs) [8–10], cavity-backed slot antennas [11–13], helical antennas [14], and microstrip antennas [15–17]. While microstrip antennas have advantages such as being low profile, low cost, and low complexity, they often suffer from a narrow axial ratio (AR) bandwidth [18]. Slot antennas are a good choice for achieving wide AR bandwidth, but their bidirectional radiation patterns result in low gain and high interference. To address this issue, different studies have proposed using metal reflectors and cavity backs [2]. For example, in [19], an artificial magnetic conductor (AMC) reflector-backed antenna was proposed, but its complex structure and decreased gain at high frequencies limit its practicality. Cavity-backed slot antennas, on the other hand, have become popular due to their promising radiation characteristics and are commonly used in communication systems [20]. Various types of CP cavity-backed antennas, such as substrate-integrated waveguide (SIW) cavities, have been reported as well [21–23].

In [2], a cavity-backed slot antenna with a square parasitic patch was proposed, which achieved a 3 dB AR bandwidth of 43.3% and a peak gain of 8.6 dB. However, the lateral dimension of this antenna is large. Another cavity-backed slot antenna was presented in [11] to enhance the gain. This antenna was implemented in a single rectangular metal cavity and had a feeding slot at the bottom to excite

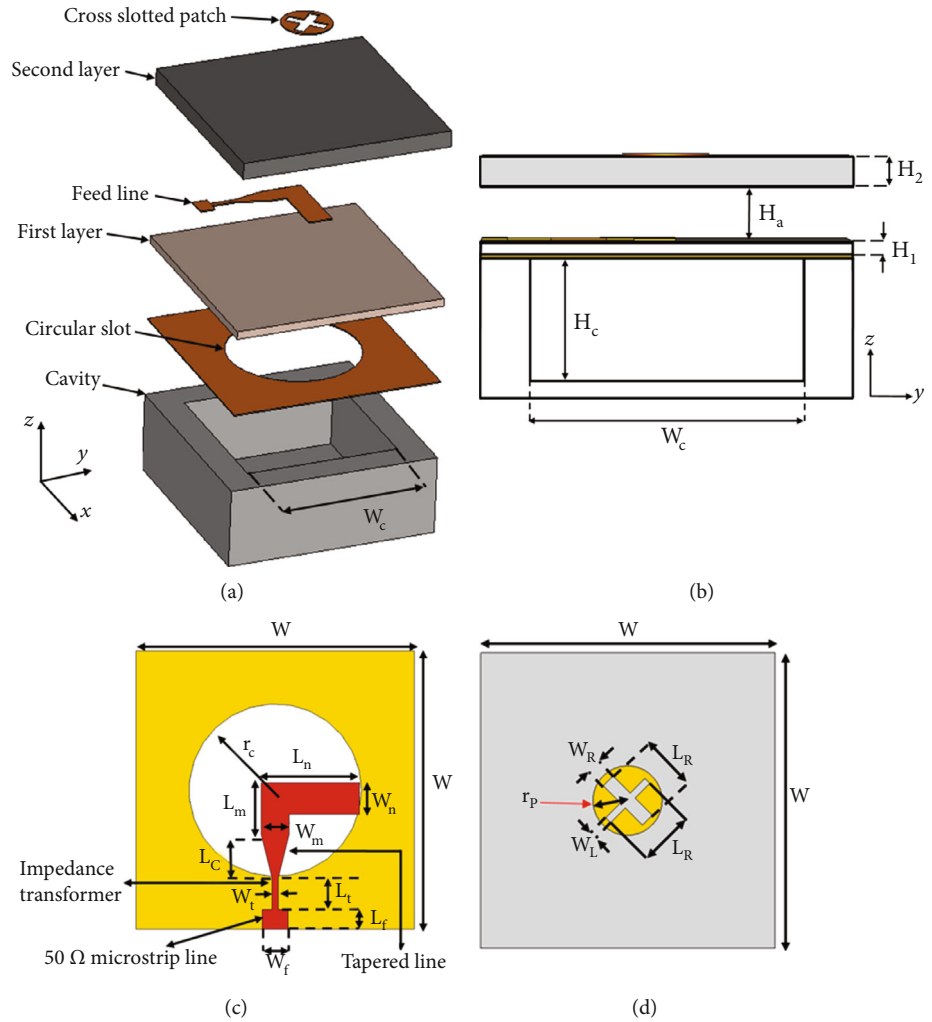

FIGURE 1: The structure of the single-element cavity-backed slot antenna: (a) 3D layout, (b) side view, (c) circular slot and its feed line on the first layer, and (d) cross-slotted circular patch on the second layer.

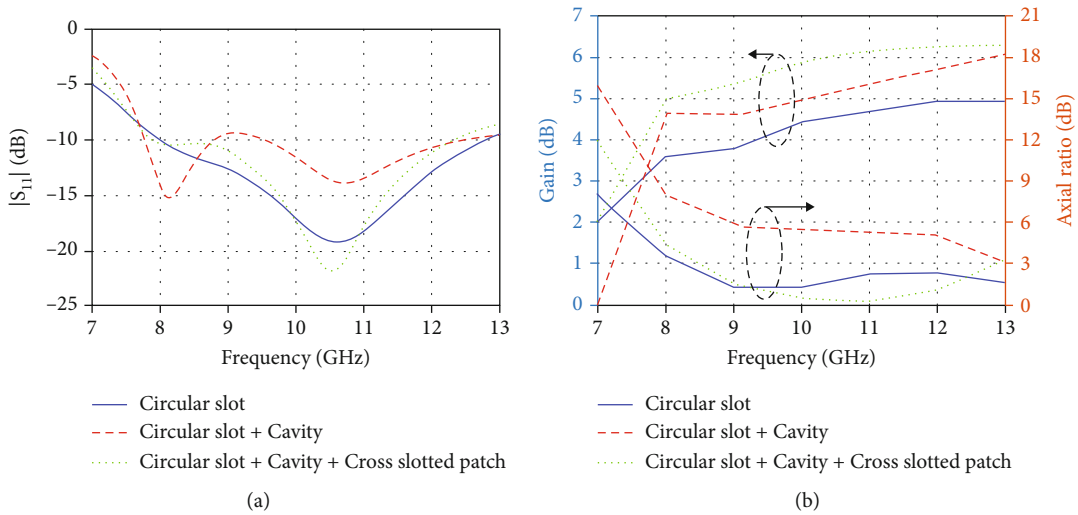

FIGURE 2: Investigation of the effects of different layers on the antenna performance: (a) reflection coefficient; (b) variation of axial ratio and gain vs. frequency at $\theta = 0^\circ$ and $\varphi = 90^\circ$.

Table 1: Dimensions of the proposed single-element antenna.

Parameter	L_f	W_f	L_t	W_t	L_C	L_m	W_m	L_R	H_a	H_1
Value (mm)	1.5	1.48	2.5	0.17	3	4	2.1	4	3.2	0.8
Parameter	r_c	W	r_p	W_R	W_L	W_c	H_c	L_n	W_n	H_2
Value (mm)	6.6	21.3	3	1	0.5	15.5	7	7.5	2.4	1.57

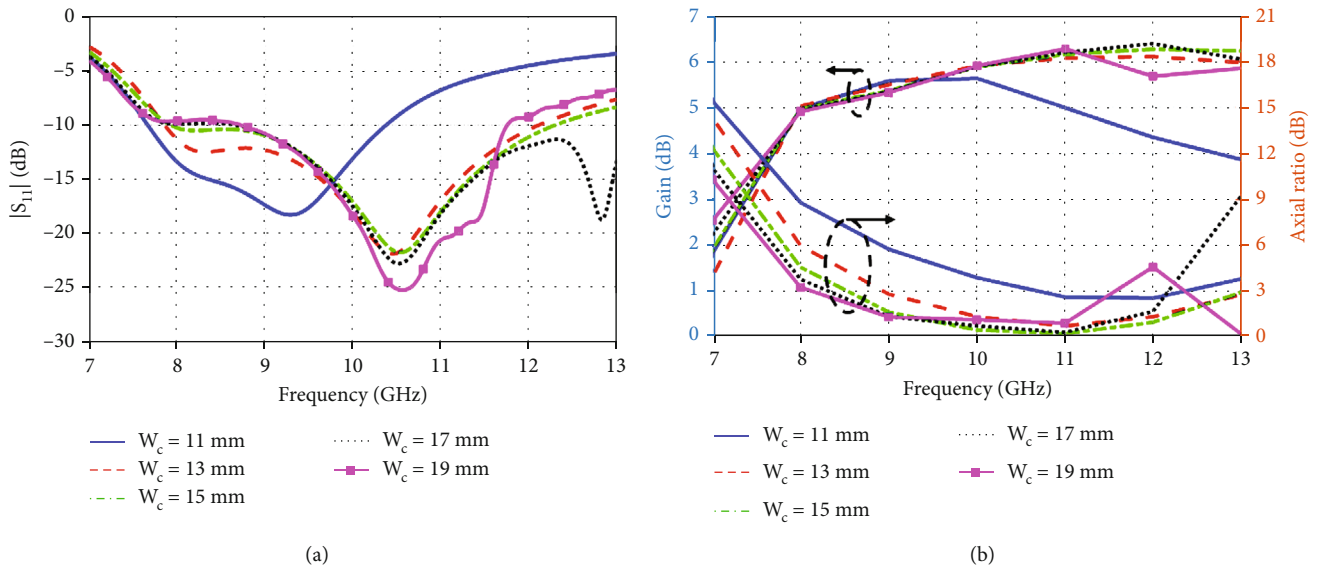

Figure 3: The effect of different values of W_c on the antenna performance: (a) reflection coefficient; (b) variation of axial ratio and gain vs. frequency at $\theta = 0^\circ$ and $\varphi = 90^\circ$.

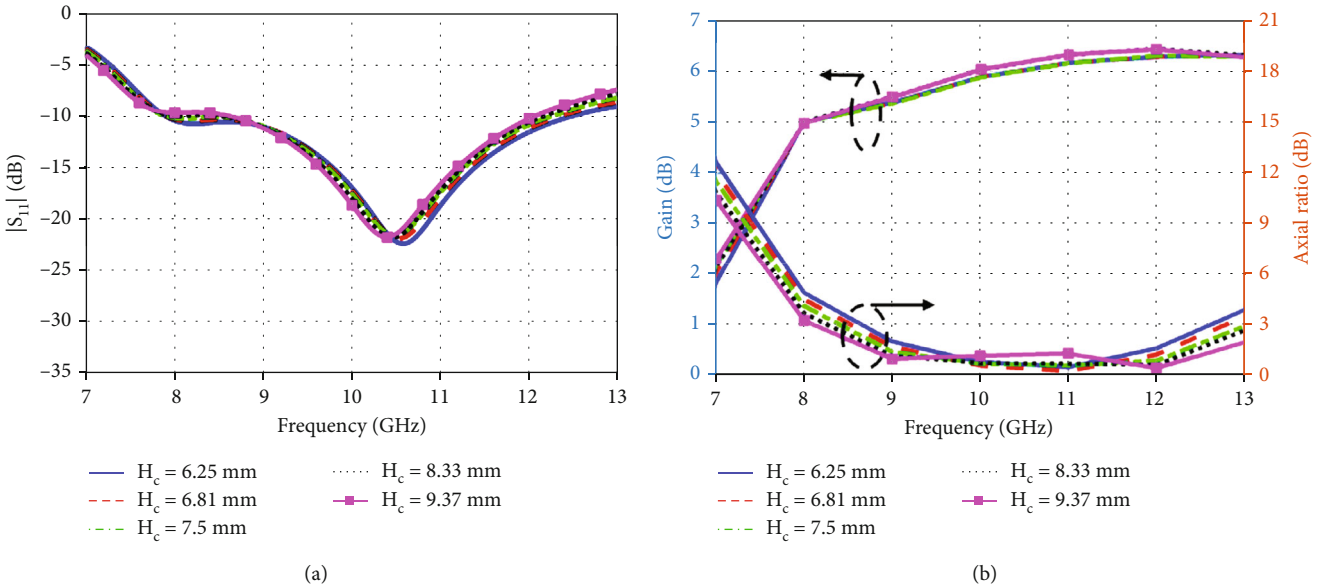

Figure 4: The effect of different values of H_c on the antenna performance: (a) reflection coefficient; (b) variation of axial ratio and gain vs. frequency at $\theta = 0^\circ$ and $\varphi = 90^\circ$.

two orthogonal resonant modes. However, the impedance and AR bandwidths of this antenna were relatively narrow, measuring approximately 6.8% and 1%, respectively. Additionally, in [13], a compact CP antenna was proposed for Internet of Things (IoT) applications. This antenna featured stubs for generating additional resonant modes in order to CP radiation. However, it had an unacceptable narrow AR bandwidth of 0.5% and a low peak gain of 2.4 dB. In [20],

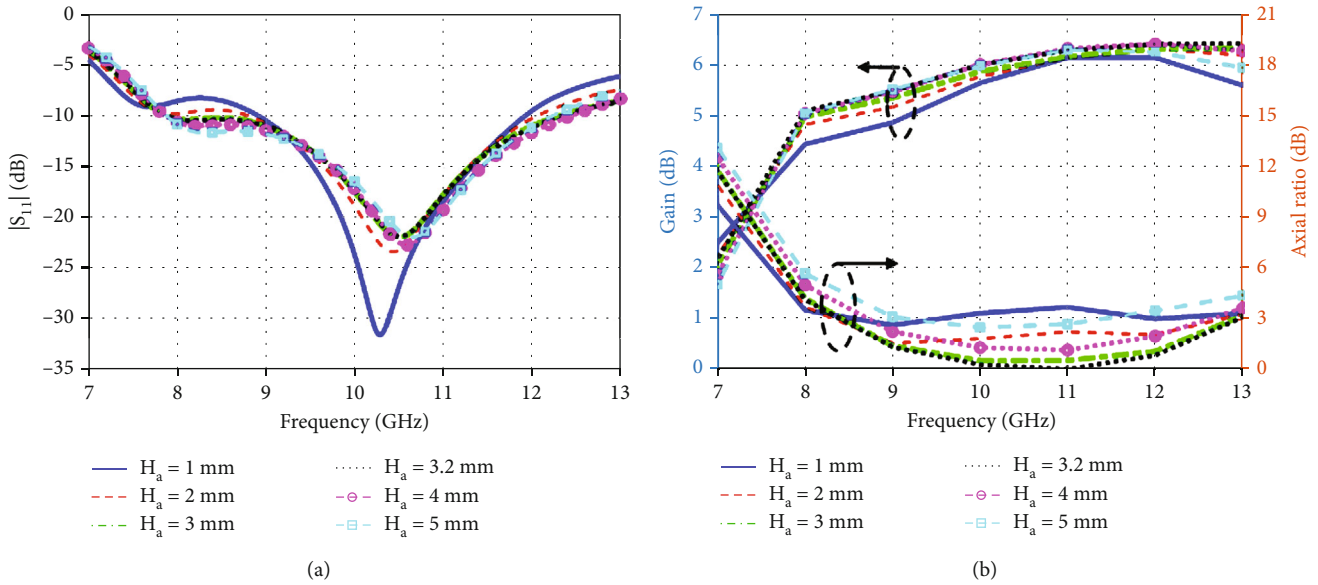

FIGURE 5: The effect of different values of H_a on the antenna performance: (a) reflection coefficient; (b) variation of axial ratio and gain vs. frequency at $\theta = 0^\circ$ and $\varphi = 90^\circ$.

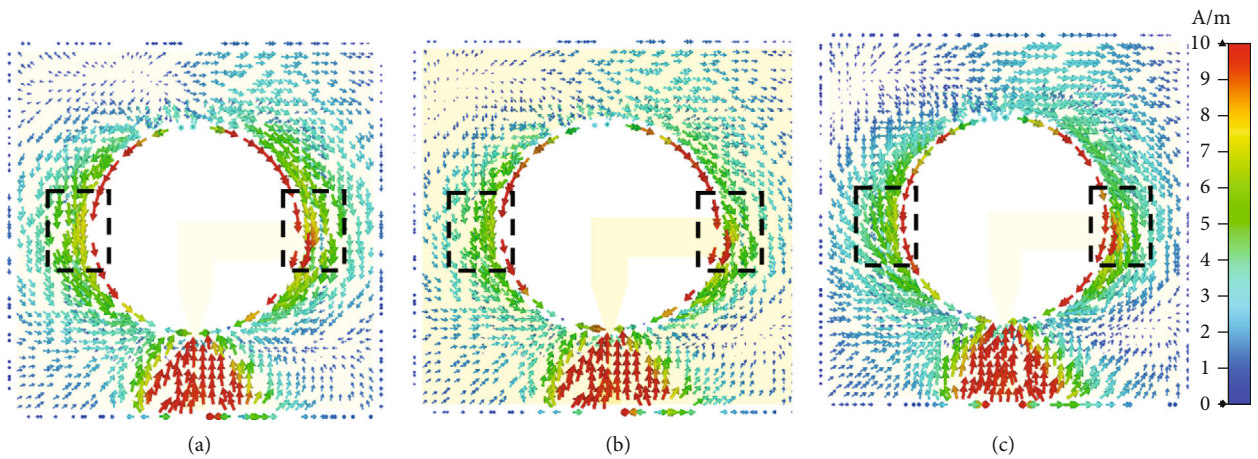

FIGURE 6: The surface current distribution on the circular slot antenna at 10 GHz: (a) without patch, (b) with patch, and (c) with patch and X slot.

a cavity-backed 2 × 2 slot antenna array based on two pairs of degenerate modes in a single cavity was proposed. This design achieved a relatively narrow AR bandwidth of 15% and a peak gain of 11.8 dB.

It is preferable to use CP array antennas instead of single-element antennas due to their wider AR bandwidth and higher gain [4]. To effectively feed the antenna elements in an array, a low complexity feed network is necessary. The sequential rotation (SR) feed network [24] is commonly used with linearly polarized patch antennas to achieve CP radiation [25]. It produces signals with equal amplitude and 90° phase difference at the output ports. It can also be used with CP antenna elements to enhance the AR bandwidth and gain, making it more suitable [26–28].

This study presents a cost-effective cavity-backed CP slot antenna array that offers high gain and wide bandwidth. The antenna design utilizes a square back cavity to increase gain and provide unidirectional radiation. To achieve CP radiation, the slot antenna is fed by a proximity-coupled L-shaped microstrip line, which excites two orthogonal modes. Additionally, a cross-slotted circular patch is incorporated at the top layer to expand the AR bandwidth, increase gain, and minimize beam squint caused by the asymmetric feed line. The single-element antenna is arranged in a 2 × 2 array configuration, and a sequential rotation feed network is utilized to achieve broader AR bandwidth and higher gain.

The structure of this paper is as follows: Section 2 presents the configuration and parametric study of the CP single-element antenna. In Section 3, the 2 × 2 antenna array with a sequential phase feed network is introduced. The simulated and measured results, along with a comparison to other similar antenna arrays, are discussed in Section 4. Finally, Section 5 presents the conclusion.

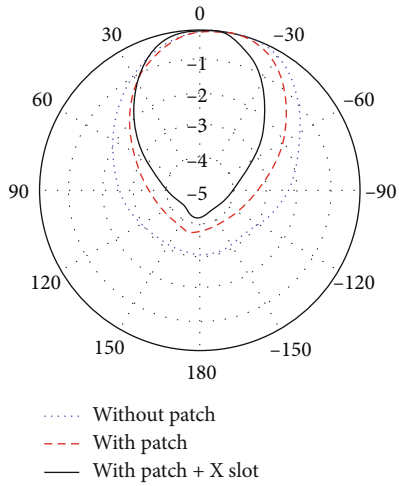

Figure 7: The normalized radiation pattern of the proposed antenna in $\varphi = 90^{\circ}$ plane for the three investigated cases at 10 GHz.

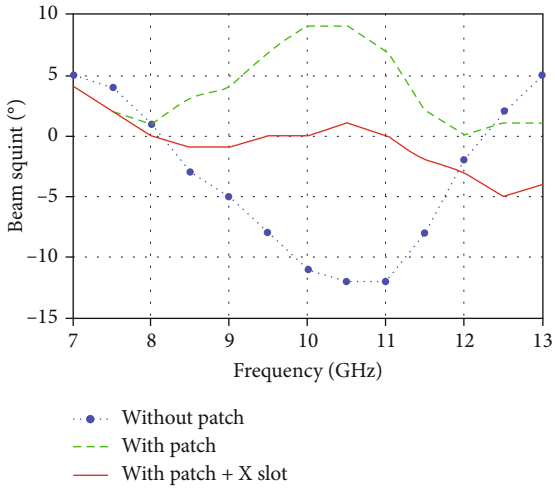

Figure 8: Variation of the beam squint angle with and without X slot.

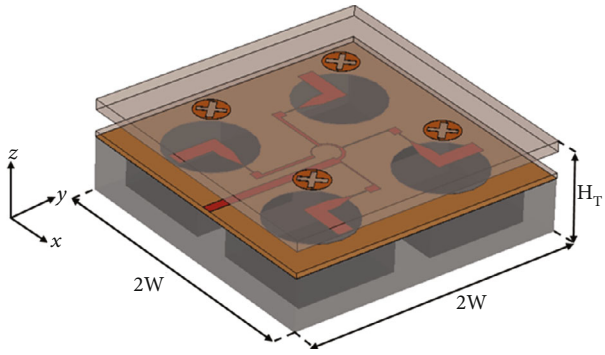

Figure 9: Geometry of the 2×2 array antenna ($W = 21.3$ mm, $H_T = 13.6$ mm).

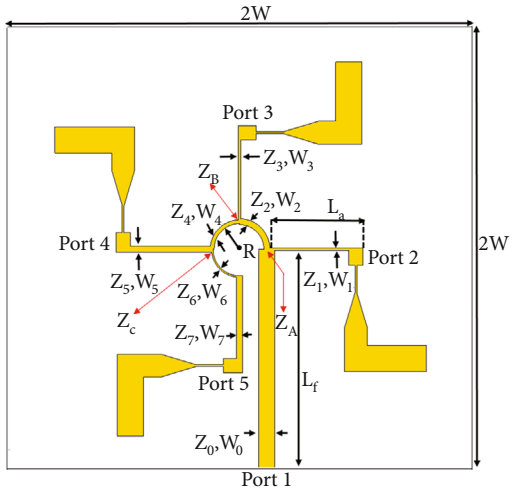

Figure 10: The sequential rotation feed network.

2. Design of the Single-Element CP Antenna

The structure of the single-element antenna is depicted in Figure 1. It comprises a low-profile cavity at the bottom, a circular slot antenna on the first layer, a cross-slotted patch on the second layer, and an air gap between two substrate layers. In the middle of the two layers, an L-shaped microstrip line is used to feed both the slot and patch antennas through proximity coupling. This feed line excites two orthogonal modes of the circular slot to achieve CP radiation. The circular slot and feed line are printed on an FR4 substrate with a thickness of 0.8 mm, $\varepsilon_r = 4.4$, and tan $\delta = 0.025$. The radius of the circular slot, denoted as "r_c" is determined approximately by [2]

$$f = \frac{1.84c}{2\pi r_c} \times \sqrt{\frac{1+\varepsilon_r}{2\varepsilon_r}}, \tag{1}$$

where c is the speed of EM waves in free space, f is the resonant frequency of the circular slot, and ε_r is the dielectric constant of the first substrate layer (FR4).

The microstrip feed line is illustrated in Figure 1(c). To mitigate the negative effects of impedance mismatching between the input 50 Ω and the L-shaped feed line, a tapered quarter-wavelength line is used as an impedance transformer. However, feeding the slot antenna with the L-shaped line introduces asymmetry in the antenna structure, leading to a squint beam in radiation patterns. To address this issue and enhance gain and AR bandwidth, a circular patch with a cross (X) slot etched on it is placed on top of the circular slot antenna. This patch is printed on an RT/duroid 5870 substrate with a thickness of 1.57 mm, $\varepsilon_r = 2.33$, and tan $\delta = 0.0009$. The unequal X slot is strategically positioned to minimize the squint angle, resulting in a symmetric radiation pattern.

In addition, to achieve a unidirectional radiation pattern, a low-profile square cavity is placed below the slot antenna. The optimized dimensions of the cavity are

Table 2: Dimensions of the sequential rotation feed network.

Parameter	L_f	W	W_0	W_1	W_2	W_3	W_4	W_5	W_6	W_7	L_a	R
Value (mm)	21.3	21.3	1.48	0.2	0.55	0.17	0.35	0.55	0.14	0.55	8.8	2.5

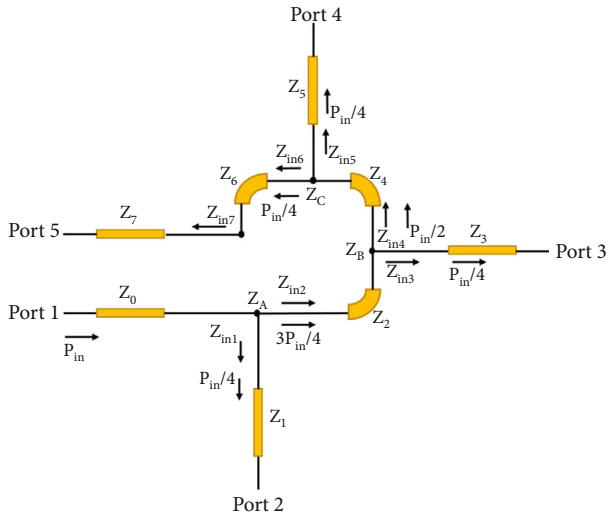

Figure 11: The equivalent circuit model of the sequential rotation feed network.

$0.5\lambda_0 \times 0.5\lambda_0 \times 0.23\lambda_0$, where λ_0 is the wavelength at the center frequency of 10 GHz. Finally, to further enhance gain and bandwidth, an air gap is included between the two layers. The thickness of air gap, represented as H_a in Figure 1(b), is carefully adjusted to be approximately $0.1\lambda_0$ (3.2 mm) for optimal performance.

Improving the impedance bandwidth and/or gain of the proposed antenna is based on the combination of several methods which have been extensively studied in the literature [29, 30]. These methods include (a) using proximity-coupled feed, (b) incorporating parasitic elements, and (c) utilizing thick substrates with low permittivity. Compared to direct feeding methods, coupling feeding methods provide a wider bandwidth. Moreover, the antenna structure consists of two resonators: a circular slot and a circular patch, each with its own resonance frequency. The patch is a gap coupled to the fed resonant circular slot antenna to provide a resonance close to the main resonance of the slot antenna. To achieve a wider bandwidth, the patch is tuned to resonate at a frequency near, but not exactly the same as, the resonance of the slot.

In addition, to improve the gain or expand the bandwidth of patch antennas, it is preferred to use substrates with greater thickness and lower dielectric constants. One approach to achieve this is by incorporating an air gap between two substrate layers, which increases overall thickness while decreasing the effective dielectric constant. However, according to [30], the relationship between gain, bandwidth, and air spacing is nonlinear. Therefore, the optimal air spacing value, which strikes a balance between higher gain and wider bandwidth, is determined through software analysis and optimization.

In terms of reflection coefficient, axial ratio (AR) level, and peak gain variation, the performance of the antenna with different layers is compared in Figure 2. The addition of the cavity improves the gain of the simple circular slot by at least 1.18 dB but degrades impedance matching and increases the AR level. On the other hand, adding the cross-slotted patch improves gain, AR level, and bandwidth that were degraded by the inclusion of the back cavity.

The proposed antenna achieves an impedance bandwidth of ~44% (7.9 GHz-12.34 GHz), with an AR below 3 dB within ~41% bandwidth (8.48 GHz-12.85 GHz). Additionally, it attains a peak gain of 6.3 dB, which is 1.37 dB higher than the circular slot antenna alone. The optimized dimensions of the antenna are provided in Table 1. It has an overall size of $0.71\lambda_0 \times 0.71\lambda_0 \times 0.45\lambda_0$.

A parametric study was also conducted to assess the impact of dimension variation on antenna performance. Specifically, the width of the cavity (W_c) was increased from 11 mm to 19 mm in 2 mm increments, while the height of the cavity (H_c) was varied between a quarter wavelength at the lowest and highest operating frequencies. The simulation results in Figures 3 and 4 were analyzed, and optimized values of 15.5 mm and 7 mm were chosen for W_c and H_c, respectively. Another critical parameter studied was the thickness of the air gap layer (H_a). The simulation analysis in Figure 5 revealed that the best performance over the desired frequency range was achieved at $H_a = 3.2$ mm.

To minimize beam squint, an additional analysis was conducted on the impact of the X slot. Figure 6 illustrates the surface currents of the circular slot with and without the patch. As shown in Figure 6(a), without the patch, asymmetrical surface currents were observed on the sides of the circular slot, resulting in a deviation of the antenna beam to the right from the broadside. The symmetrical patch did not significantly affect the current distribution, as shown in Figure 6(b). However, after adding the X slot on the patch, a symmetrical surface current distribution was observed with almost identical amplitude on both sides, as shown in Figure 6(c), resulting in a reduction in beam squint.

The normalized 2D radiation patterns for the three cases are displayed in Figure 7. These patterns are displayed in linear scale to enhance visibility of the beam squint. In Figure 8, the variation of beam squint is depicted versus frequency within the desired bandwidth. Implementing the X slot on the patch greatly reduces the beam squint, achieving a range of -3° to 1° over the bandwidth of 8 GHz to 12 GHz.

3. Antenna Array Design

3.1. 2 × 2Array. The proposed antenna is configured in a 2 × 2 array, incorporating a sequential rotation feed network to increase the gain, as well as improve the AR level and bandwidth. The simulation of the array was conducted using

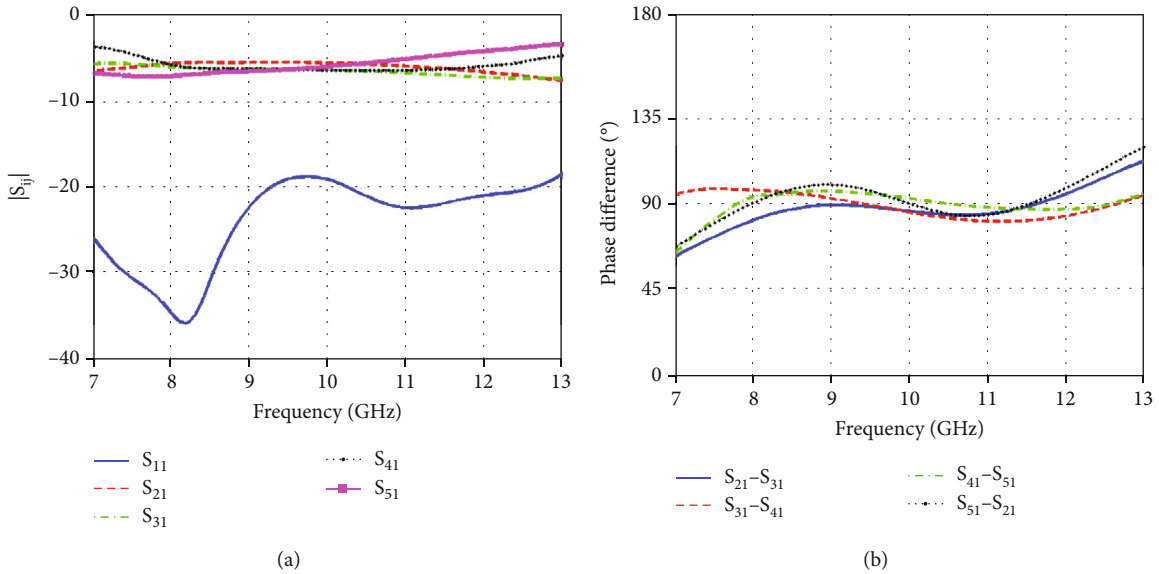

Figure 12: The simulated S-parameters and phase difference of the sequential-phase feed network.

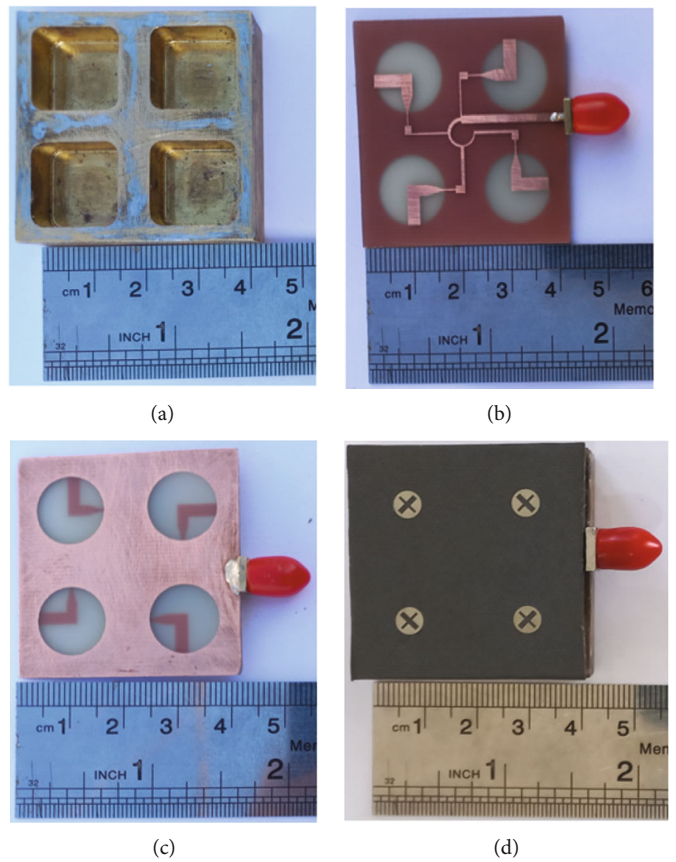

Figure 13: The fabricated 2 × 2 array antenna: (a) cavity, (b) SR feed network, (c) Circular slot antenna elements, and (d) full array antenna.

HFSS software and is depicted in Figure 9. The overall dimensions of the array are 42.6 mm × 42.6 mm × 13.6 mm.

3.2. Sequential Rotation Feed Network. Figure 10 illustrates the sequential rotation feed network used in the array, which utilizes a combination of series and parallel feed lines to interconnect the array elements. To ensure equal distribution of input power among the output ports, transmission lines with varying impedances are employed. By rotating each element sequentially with an appropriate offset in the

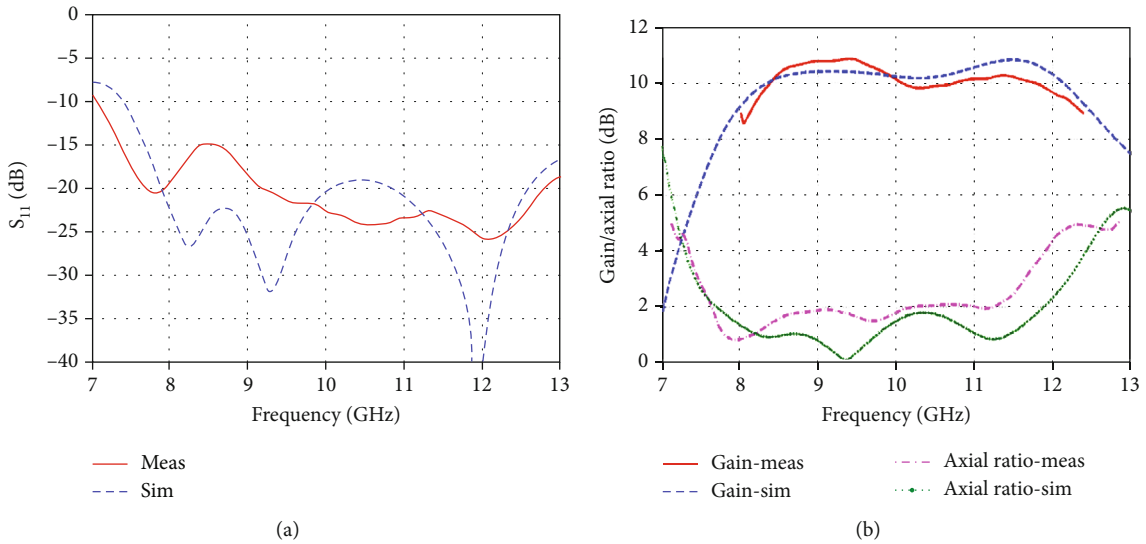

FIGURE 14: The simulated and measured results: (a) reflection coefficient; (b) variation of the gain and AR at $\theta = 0^{\circ}$ and $\varphi = 90^{\circ}$.

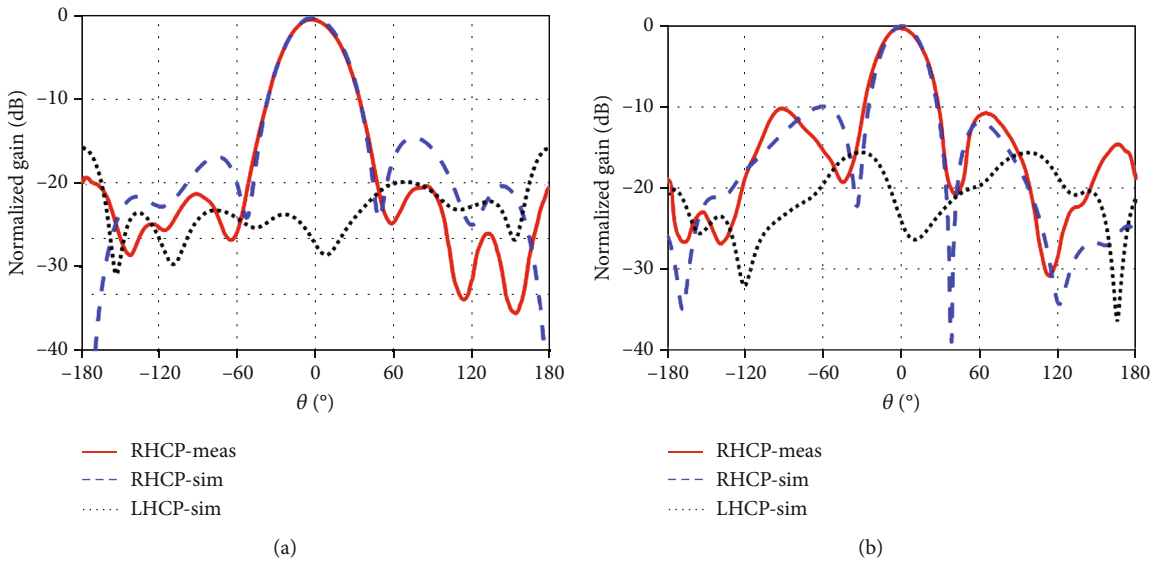

FIGURE 15: The simulated and measured normalized radiation patterns at two different frequencies: (a) 9 GHz; (b) 11 GHz.

feed excitation phase, significant improvements in both AR bandwidth and impedance bandwidth have been achieved. The feed network comprises a 270° annular sector and four quarter-wavelength impedance transformers that are sequentially rotated. These transformers have different characteristic impedances with a length of "L_a." The annular disk is composed of three quarter-wavelength sectors with varying thicknesses, which are utilized to transform the impedance between the junction points of the feed network and provide a 90° phase difference between adjacent elements. To achieve a wider bandwidth, the lengths and widths of the feed network have been optimized. Table 2 presents the parameters of the feed network.

Figure 11 illustrates the equivalent circuit model of the feed network. The input power flow to the circuit is denoted by P_{in}, which is distributed evenly among the output ports with $P_{in}/4$ per branch of the SR feed. The impedances of the sectors (Z_2, Z_4, and Z_6) are crucial for achieving sequential phase at the outputs. Optimal lengths and widths of all the branches must be determined to ensure equal power distribution across the output ports. The impedances of the output ports, Z_{p2} to Z_{p5}, and the input port, Z_0, are 50 Ω. The junction points connected to the antennas' feed lines have equivalent impedance denoted by Z_A, Z_B, and Z_C. Furthermore, the characteristic impedances of the quarter-wavelength transformers are represented as Z_1 to Z_7 and can be calculated using transmission line theory as follows [31]:

$$
\begin{aligned}
Z_A &= Z_{in1} \| Z_{in2}, \\
Z_B &= Z_{in3} \| Z_{in4}, \\
Z_C &= Z_{in5} \| Z_{in6}, \\
Z_{in7} &= \frac{Z_7^2}{Z_{P5}}, \\
Z_{in6} &= \frac{Z_6^2}{Z_{in7}}, \\
Z_{in5} &= \frac{Z_5^2}{Z_{P4}}, \\
Z_{in4} &= \frac{Z_4^2}{Z_C}, \\
Z_{in3} &= \frac{Z_3^2}{Z_{P3}}, \\
Z_{in2} &= \frac{Z_2^2}{Z_B}, \\
Z_{in1} &= \frac{Z_1^2}{Z_{P2}}.
\end{aligned} \tag{2}
$$

To equally divide the input power between four output ports, the following relations should be satisfied in the junction points:

$$
\begin{aligned}
Z_{in1} &= 3Z_{in2}, \\
Z_{in3} &= 2Z_{in4}, \\
Z_{in5} &= Z_{in6}.
\end{aligned} \tag{3}
$$

The optimal characteristic impedances of lines are as follows:

$$
\begin{aligned}
Z_1 &= 116\,\Omega, \\
Z_2 &= 81\,\Omega, \\
Z_3 &= 120\,\Omega, \\
Z_4 &= 96\,\Omega, \\
Z_5 &= 81\,\Omega, \\
Z_6 &= 127\,\Omega, \\
Z_7 &= 81\,\Omega.
\end{aligned} \tag{4}
$$

Figures 12(a) and 12(b) illustrate the simulated S-parameters and phase difference between the output ports of the feed network, respectively. The input reflection coefficient is below -19 dB over the desired frequency range of 8 GHz-12 GHz, indicating good impedance matching. Furthermore, $|S_{21}|$, $|S_{31}|$, $|S_{41}|$, and $|S_{51}|$ exhibit values close to -6 dB with a maximum amplitude imbalance of ±0.6 dB. The phase differences between ports are $-90^\circ \pm 5^\circ$, which is necessary to achieve RHCP radiation over 8 GHz-12 GHz. However, it should be noted that the amplitude and phase of the output signals will be further optimized when the feed network is connected to the antenna elements, taking into account the effects of coupling.

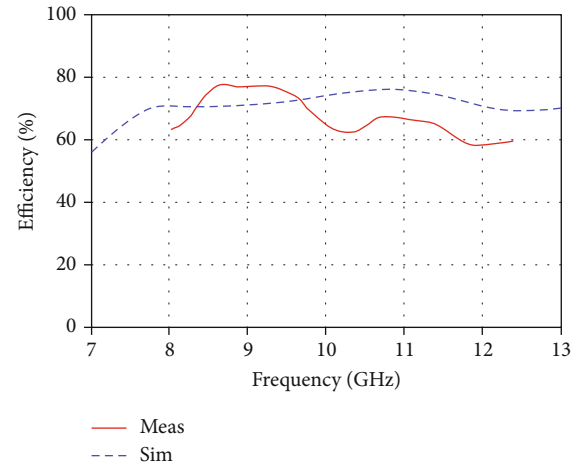

Figure 16: The simulated and measured efficiency vs. frequency.

Table 3: Comparison of the proposed antenna array characteristics with recent works in 2 × 2 configurations.

Antenna	Size (λ_0^3)	Impedance bandwidth (%)	3 dB AR bandwidth (%)	Peak gain (dB)
[20]	1.3 × 1.3 × 0.85	19	15	11.8
[32]	1.64 × 1.64 × 2.07	40.3	40.3	16.3
[33]	3.02 × 3.02 × 0.08	13.1	7.2	10.9
[34]	1.88 × 1.88 × 0.51	70	50	11
This work	1.42 × 1.42 × 0.45	60	42	11.14

4. Simulated and Measured Results of the Array Antenna

To validate the performance of the design, the array antenna was fabricated and tested. Figure 13 shows the different layers of the array both before and after assembly. The measured reflection coefficient of the array is compared to the simulation in Figure 14(a). The impedance bandwidth, with $|S_{11}| < -10$ dB, is 60%, covering the frequency range of 7 GHz-13 GHz. In addition, Figure 14(b) illustrates the variation of the measured peak gain and AR versus frequency. The 3 dB AR bandwidth is 42% (7.45 GHz-11.65 GHz), and the maximum gain is 11.14 dB.

In Figures 15(a) and 15(b), the simulated and measured normalized co-pol. (RHCP) and cross-pol. (LHCP) components of the radiation patterns are compared at 9 GHz and 11 GHz, respectively. The radiation patterns exhibit symmetry, and the side lobe levels (SLL) are below -20 dB and -10 dB, respectively, at 9 GHz and 11 GHz. Figure 16 presents the simulated and measured efficiency of the array,

indicating a total efficiency exceeding 60% across the desired bandwidth of 40% (8 GHz-12 GHz).

Table 3 presents a comparison between the proposed array antenna and previously reported arrays in literature with a 2×2 configuration. The results demonstrate that the proposed antenna array has smaller dimensions compared to those presented in [32–34]. Additionally, the impedance bandwidth and AR bandwidth are superior to [20, 32, 33]. Although the peak gain is lower than [20, 32], the smaller size of the proposed array is also noteworthy.

5. Conclusion

In this study, a broadband 2×2 cavity-backed circularly polarized (CP) slot antenna array is proposed for X-band applications. The array utilizes a sequential rotation feed network and incorporates a low-profile cavity and a cross-slotted patch into the circular slot antenna to improve the gain and widen the impedance and AR bandwidths. With $|S_{11}| \leq -10$ dB, the array covers frequencies from 7 GHz to 13 GHz, and the AR is lower than 3 dB over the frequency range of 7.45 GHz-11.65 GHz. Measured results show a peak gain of 11.14 dB and an SLL lower than -10 dB throughout the desired frequency range, making this antenna array suitable for use in radar and satellite communication systems.

Data Availability

The datasets generated in this study are available from the authors on reasonable request.

Conflicts of Interest

The authors declare that they have no conflicts of interest.

References

[1] Y. Zou, H. Li, Y. Xue, and B. Sun, "A high-gain compact circularly polarized microstrip array antenna with simplified feed network," *International Journal of RF and Microwave Computer-Aided Engineering*, vol. 29, no. 12, article e21964, 2019.

[2] W. Yang and J. Zhou, "Wideband circularly polarized cavity backed aperture antenna with a parasitic square patch," *IEEE Antennas and Wireless Propagation Letters*, vol. 13, pp. 197–200, 2014.

[3] D. Cheng, M. Chen, and L. Tian, "Low-cost and wideband circularly polarized slot antenna array," *International Journal of RF and Microwave Computer-Aided Engineering*, vol. 30, no. 9, article e22316, 2020.

[4] H. Xu, J. Zhou, K. Zhou, Q. Wu, Z. Yu, and W. Hong, "Planar wideband circularly polarized cavity-backed stacked patch antenna array for millimeter-wave applications," *IEEE Transactions on Antennas and Propagation*, vol. 66, no. 10, pp. 5170–5179, 2018.

[5] S. Gao, Q. Luo, and F. Zhu, *Circularly Polarized Antennas*, John Wiley & Sons, New Jersey, 1st edition, 2014.

[6] M. Nosrati, C. Yang, X. Liu, and N. Tavassolian, "Wideband circularly polarized slot antenna array loaded with metasurface," *Microwave and Optical Technology Letters*, vol. 62, no. 9, pp. 2976–2988, 2020.

[7] K. Luo, B. Chen, and W. P. Ding, "Meander line coupled cavity-backed slot antenna for broadband circular polarization," *IEEE Antennas and Wireless Propagation Letters*, vol. 14, pp. 1215–1218, 2015.

[8] R. Chowdhury and R. K. Chaudhary, "Investigation on different forms of circular sectored-dielectric resonator antenna for improvement in circular polarization performance," *IEEE Transactions on Antennas and Propagation*, vol. 66, no. 10, pp. 5596–5601, 2018.

[9] L. Wang, S. W. Wong, X. Zhang et al., "Stable high-gain linearly and circularly polarized dielectric resonator antennas based on multiple high-order modes," *IEEE Transactions on Antennas and Propagation*, vol. 70, no. 12, pp. 12270–12275, 2022.

[10] R. Chowdhury and R. K. Chaudhary, "An approach to generate circular polarization in a modified cylindrical shaped dielectric resonator antenna using PMC boundary approximation," *IEEE Antennas and Wireless Propagation Letters*, vol. 17, no. 9, pp. 1727–1731, 2018.

[11] Y. M. Wu, S. W. Wong, J. Y. Lin, L. Zhu, Y. He, and F. C. Chen, "A circularly polarized cavity-backed slot antenna with enhanced radiation gain," *IEEE Antennas and Wireless Propagation Letters*, vol. 17, no. 6, pp. 1010–1014, 2018.

[12] M. H. Hoang, T. Q. V. Hoang, H. P. Phan, and T. P. Vuong, "Cavity-backed circular-polarized compact slot antenna for handheld UHF RFID reader," *IEEE Antennas and Wireless Propagation Letters*, vol. 14, pp. 1439–1442, 2015.

[13] J. I. Oh, H. W. Jo, K. S. Kim, H. Cho, and J. W. Yu, "A compact cavity-backed slot antenna using dual mode for IoT applications," *IEEE Antennas and Wireless Propagation Letters*, vol. 20, no. 3, pp. 317–321, 2021.

[14] Z. Chen and Z. Shen, "Planar helical antenna of circular polarization," *IEEE Antennas and Wireless Propagation Letters*, vol. 63, no. 10, pp. 4315–4323, 2015.

[15] M. Elahi, S. T. Van, Y. Yang, K. Y. Lee, and K. C. Hwang, "Compact and high gain 4×4 circularly polarized microstrip patch antenna array for next generation small satellite," *Applied Sciences*, vol. 11, no. 19, p. 8869, 2021.

[16] L. Wang and Y. F. En, "A wideband circularly polarized microstrip antenna with multiple modes," *IEEE Open Journal of Antennas and Propagation*, vol. 1, pp. 413–418, 2020.

[17] C. Deng, Y. Li, Z. Zhang, and Z. Feng, "A wideband sequential-phase fed circularly polarized patch array," *IEEE Transactions on Antennas and Propagation*, vol. 62, no. 7, pp. 3890–3893, 2014.

[18] X. Jiang, Z. Zhang, Y. Li, and Z. Feng, "A low-cost wideband circularly polarized slot array with integrated feeding network and reduced height," *IEEE Transactions on Antennas and Propagation*, vol. 15, pp. 222–225, 2015.

[19] K. Agarwal and A. Alphones, "Wideband circularly polarized AMC reflector backed aperture antenna," *IEEE Transactions on Antennas and Propagation*, vol. 61, no. 3, pp. 1456–1461, 2013.

[20] R. S. Chen, G. L. Huang, S. W. Wong, M. K. T. Al-Nuaimi, K. W. Tam, and W. Choi, "Bandwidth-enhanced circularly polarized slot antenna and array under two pairs of degenerate modes in a single resonant cavity," *IEEE Antennas and Wireless Propagation Letters*, vol. 22, no. 2, pp. 288–292, 2023.

[21] D. F. Guan, C. Ding, Z. P. Qian, Y. S. Zhang, Y. J. Guo, and K. Gong, "Broadband high-gain SIW cavity-backed circular-polarized array antenna," *IEEE Antennas and Wireless Propagation Letters*, vol. 64, no. 4, pp. 1493–1497, 2016.

[22] H. Gharibi and F. H. Kashani, "Design of a compact high-efficiency circularly polarized monopulse cavity-backed substrate integrated waveguide antenna," *IEEE Antennas and Wireless Propagation Letters*, vol. 63, no. 9, pp. 4250–4256, 2015.

[23] W. Li, X. H. Tang, and Y. Yang, "A Ka-band circularly polarized substrate integrated cavity-backed antenna array," *IEEE Antennas and Wireless Propagation Letters*, vol. 18, no. 9, pp. 1882–1886, 2019.

[24] S. X. Ta and I. Park, "Planar wideband circularly polarized metasurface based antenna array," *Journal of Electromagnetic Waves and Applications*, vol. 30, no. 12, pp. 1620–1630, 2016.

[25] H. Evans, P. Gale, B. Aljibouri, E. G. Lim, E. Korolkeiwicz, and A. Sambell, "Application of simulated annealing to design of serial feed sequentially rotated 2 × 2 antenna array," *Electronics Letters*, vol. 36, no. 24, pp. 1987-1988, 2000.

[26] V. Rafii, J. Nourinia, C. Ghobadi, J. Pourahmadazar, and B. S. Virdee, "Broadband circularly polarized slot antenna array using sequentially rotated technique for C-band applications," *IEEE Antennas and Wireless Propagation Letters*, vol. 12, pp. 128–131, 2013.

[27] S. Mohammadi-Asl, J. Nourinia, C. Ghobadi, and M. Majidzadeh, "Wideband compact circularly polarized sequentially rotated array antenna with sequential-phase feed network," *IEEE Antennas and Wireless Propagation Letters*, vol. 16, pp. 3176–3179, 2017.

[28] W. Yang, J. Zhou, Z. Yu, and L. Li, "Bandwidth-and gain-enhanced circularly polarized antenna array using sequential phase feed," *IEEE Antennas and Wireless Propagation Letters*, vol. 13, pp. 1215–1218, 2014.

[29] K. F. Lee, K. M. Luk, and H. W. Lai, *Microstrip Patch Antennas*, World Scientific, 2nd edition, 2017.

[30] R. Q. Lee, K. F. Lee, and J. Bobinchak, "Characteristics of a two-layer electromagnetically coupled rectangular patch antenna," *Electronics Letters*, vol. 23, no. 20, pp. 1070–1072, 1987.

[31] C. A. Balanis, *Antenna Theory: Analysis and Design*, John Wiley & Sons, New Jersey, 3rd edition, 2005.

[32] J. Wu, C. Wang, and Y. Guo, "A wideband circularly polarized array antenna with compact and high-efficiency feeding network," *IEEE Transactions on Antennas and Propagation*, vol. 68, no. 1, pp. 62–69, 2020.

[33] E. Y. Jung, J. W. Lee, T. K. Lee, and W. K. Lee, "SIW-based array antennas with sequential feeding for X-band satellite communication," *IEEE Transactions on Antennas and Propagation*, vol. 60, no. 8, pp. 3632–3639, 2012.

[34] K. F. Hung and Y. C. Lin, "Novel broadband circularly polarized cavity-backed aperture antenna with traveling wave excitation," *IEEE Transactions on Antennas and Propagation*, vol. 58, no. 1, pp. 35–42, 2010.